DOI: 10.61782/fa.2025.0195

FORUM ACUSTICUM
EURONOISE 2025

CHARACTERIZATION OF PLANAR CIRCULAR AND SQUARE MEMS MICROPHONE ARRAYS FOR LOW-POWER ACOUSTIC APPLICATIONS

Ricardo Moreno[1*] **Jorge Ortigoso-Narro**[2] **Marco Raiola**[1]
Luis A. Azpicueta-Ruiz[2] **Daniel de la Prida**[3]

[1] Department of Aerospace Engineering, Universidad Carlos III de Madrid, Spain
[2] Department of Signal Theory, Universidad Carlos III de Madrid, Spain
[3] Grupo de Investigación en Acústica Arquitectónica, Universidad Politécnica de Madrid, Madrid, Spain

ABSTRACT

Advancements in microphone arrays are transforming acoustic sensing and innovating applications such as speech enhancement, beamforming, source localization, and environmental noise monitoring. On the way to developing low-cost phased arrays with numerous sensors, MEMS microphones have become a preferred solution whose distribution and positioning can boost their acoustic capabilities. The performance of both circular concentric and square grid geometries is characterized. A square grid array prioritizes low-cost scalability for high-efficiency data acquisition, while the circular concentric design optimizes directivity. Both compared arrays use the same MEMS microphone model and electronic configuration, but differ in the number of elements and aperture size. The microphone model used for both arrays allows using Time-Division Multiplexing for streamlined data collection through a single data line with an I^2S interface and integrated PCB design. The frequency response, directivity, and data transfer efficiency are analyzed by conducting experiments with a sound source at various positions within an anechoic chamber. The results demonstrate trade-offs between geometric configurations, providing valuable insight into the design of low-power, flexible, and scalable acoustic sensing systems.

*__Corresponding author__: jonmoren@ing.uc3m.es.

Keywords: *MEMS, Phased Microphone Arrays, Time-Division Multiplexing, Inter-IC Sound*

1. INTRODUCTION

The growing demand for low-cost and scalable acoustic sensing systems has fueled advancements in microphone array technology. These arrays are essential tools for applications such as noise source identification, beamforming, and environmental noise monitoring [1, 2]. Among the available technology solutions, MEMS (Micro-Electro-Mechanical Systems) microphones have gained prominence due to their reduced and compact size, low-power consumption, affordability, and integration versatility with development boards. The ease of deployment in various geometric configurations significantly influences the array's spatial resolution, directivity, and overall performance.

A critical challenge in developing massive acoustic cameras is optimizing the microphone distribution while ensuring efficient data capturing [3]. To diagnose noise generation, expensive FPGA-based acquisition systems commonly use the Inter-IC Sound (I^2S) protocol. However, standard I^2S interfaces can only support up to two microphone channels per data line, requiring multiple physical connections for larger arrays [4]. To address this limitation, the Time-Division Multiplexing (TDM) interface extends I^2S capabilities by allowing up to 16 microphone channels to be transmitted on a single data line. Thus, the number of connections can be significantly reduced, streamlining system integration and enabling a cost-effective and scalable architecture. By using

a multiplexed acquisition system, we can systematically assess the performance of different microphone distributions while ensuring consistency in sensor characteristics.

To evaluate the impact of these configurations, we compare two distinct microphone array geometries: a circular concentric array CCA and a square grid array SGA. Both arrays utilize the same MEMS microphone model and electronic setup, differing only in their spatial arrangement, number of elements, and aperture. These configurations are designed as a complete acquisition system intended for use with a low-cost microprocessor development board. The acquired signals must undergo post-processing after acquisition, meaning that all analyses are conducted offline. As it can be seen in Fig. 1, the CCA features a completely solid design, whereas the SGA distributes its microphones along a grid structure, and therfore is expected to behave more transparently concerning wave incidence.

Experiments in this study focus on analyzing the frequency response of each microphone within both array configurations to determine potential variations across the array, and also considering different orientations with respect to the noise source, i.e., the array directivity. Additionally, we assessed whether the multiplexing process impacts measurement accuracy. To demonstrate the synchronization of the multiplexed system, we evaluate its functionality with the worst-case scenario (SGA), where signals are stressed at the maximum trace length recommended by the manufacturer and the one that multiplexes the maximum number of channels supported. These results will provide insights into the reliability of TDM acquisition for scalable, low-power microphone arrays and contribute to optimizing array design for acoustic sensing applications.

The breakout of this document is as follows: Section 2 describes the design of both microphone arrays, explaining the criteria behind their geometries and detailing the composition of the acquisition system. Section 3 outlines the methodology used to evaluate their performance, focusing on three key aspects: frequency response, directivity, and TDM synchronization. In Section 4, the results of these evaluations are presented, supported by graphs and performance parameters. Finally, Section 5 provides a discussion of the findings and summarizes the main conclusions of this work.

2. MICROPHONE ARRAY DESIGNS

2.1 Hardware Development

The modular SGA design has been explained in detail in [5]. Such array follows a scalable architecture consisting of four identical modules, each containing 16 daisy-chain microphones model ICS-52000 [6]. For this study, we assessed the performance of one 16-microphone submodule. Microphones of this array design are evenly spaced and arranged in a 4×4 square grid, with $62.5\,\mathrm{mm}$ between adjacent microphones. To minimize propagation delay mismatches, all electrical connections adhere strictly to the manufacturer's recommendations, with trace lengths set to the maximum allowable limits and matched impedance at clock frequency.

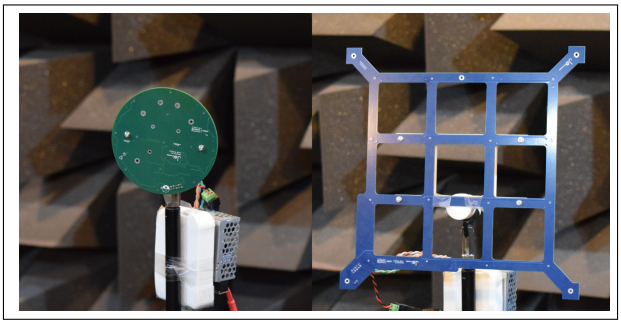

Figure 1. On the left-hand side, the CCA composed of 13 MEMS microphones. The blue printed circuit board corresponds to the SGA with 16 microphones distributed in a Cartesian grid.

Beyond electrical considerations, the SGA's mechanical design was developed to be minimally intrusive to the test environment, reducing the risk of potential airborne disturbances. The printed circuit board occupies a considerable surface area, which could reflect sound energy and introduce pressure variations that degrade acoustic measurements. To counteract this, sections of the structure between microphones have been removed, allowing air to pass freely through the array. This design choice minimizes reflections and potential aerodynamic artifacts. By balancing electrical, spatial, and mechanical constraints, this microphone array optimizes acoustic performance and modular scalability. Moreover, if this microphone array design were used for beamforming applications, its aperture size and microphone separation would impose limitations, e.g., reduced spatial resolution and grating lobes generation, for frequencies under

$f_L \approx 1\,\mathrm{kHz}$ and above $f_H \approx 2.7\,\mathrm{kHz}$, respectively.

A different approach is observed in the CCA, which consists of 13 microphones: one at the center, four distributed along a $2.5\,\mathrm{cm}$ radius, and eight along a $4.5\,\mathrm{cm}$ radius. Compared to SGA from a theoretical point of view, the microphone distribution of this CCA would offer improved directionality and isotropic coverage, making it more suitable for applications requiring omnidirectional sound capture and robust source localization [7], although it is expected that its solid design will affect the directivity in the high frequency range. Furthermore, due to its short and non-uniform spacing, the array may introduce more spatial aliasing effects depending on the frequency range of interest. Additionally, its smaller aperture limits its ability to resolve lower frequency sources as effectively as the larger square array. For this setup, the approximate lower and upper frequency bounds are $f_L \approx 3.8\,\mathrm{kHz}$ and $f_H \approx 8.5\,\mathrm{kHz}$, respectively.

2.2 Data Transmission to BeagleBone Black Board

To handle the signal acquisition, a BeagleBone Black board (BBB) was chosen as the main processing unit. The primary reason for this selection was its Multichannel Audio Serial Port (McASP), which enables seamless interfacing with TDM digital audio streams. Since the MEMS microphones used in both designs output data via this protocol, the acquisition system must be capable of demultiplexing the interleaved audio channels correctly. The BBB, running a Linux-based system, provided this capability while allowing efficient real-time data acquisition.

This transmission format implies that the board manages precisely a bit clock (BCK) and frame synchronization (FS) signals. The data transfer rate is defined by BCK, while FS triggers the start of the first microphone. This means that the following microphone has to wait until the first microphone finishes writing a 32-bit word and commands the word select output (WSO), as shown in Fig. 2.

For a fair comparison between both microphone arrays, the acquisition system was configured to record 16 channels at a sample frequency of $8\,\mathrm{kHz}$. In the case of the 13-microphone CCA, the last three channels were ignored during processing.

3. MEASUREMENT PROCEDURES

Measurements were carried out in an anechoic chamber to ensure a controlled acoustic environment, free from unwanted reflections and external noise. This facility is located at the Signal Theory and Communications Department of the University Carlos III de Madrid. The chamber's interior dimensions of $6.5\,\mathrm{m} \times 4.5\,\mathrm{m} \times 3.85\,\mathrm{m}$, combined with $60\,\mathrm{cm}$-long absorbing wedges, effectively attenuate reflections across a wide frequency range.

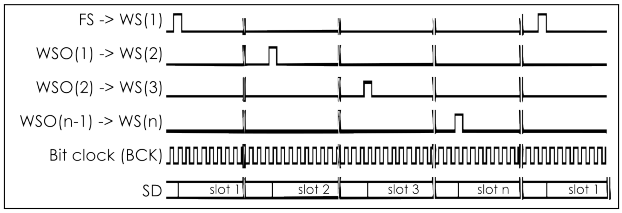

Figure 2. In the microphone datasheet, the terminology describes the Word Select (WS) and Word Select Output (WSO) as the propagation of the Frame Sync (FS) throughout the daisy-chain system. This pulse triggers the bit writing of each microphone to the Serial Data line (SD) at the Bit Clock rate (BCK), sequentially.

3.1 Frequency Response

The frequency response of both microphone arrays was evaluated following two distinct procedures, both using a domestic speaker as a sound source, specifically an Alexa Echo Pop, and generating a white noise signal.

In the first procedure, each microphone was assessed individually at a distance of $1\,\mathrm{m}$ from the sound source. The objective of this measure was to compare the magnitude of the frequency response of each microphone when positioned at the same location relative to the source. To achieve precise positioning, a cross-line laser was used to mark the exact spot on each microphone, always keeping the 1-meter distance throughout the procedure, as shown in Fig. 3. Measurements were conducted sequentially, displacing the arrays in a parallel plane to the source position, and ensuring that only the channel that corresponds to the microphone positioned at the spot is analyzed at a time.

We calculate the deviation in the frequency response of the i-th microphone using $\Delta H_i(f)$ as figure of merit, denoted as

$$\Delta H_i(f) = H_i(f)\ (\mathrm{dB}) - H_{\mathrm{av}}(f)\ (\mathrm{dB}), \qquad (1)$$

where $H_i(f)$ represents the magnitude of the i-th microphone in decibels, and $H_{\mathrm{av}}(f)$ is the reference value to compare, obtained as the average of all the frequency re-

sponses magnitudes across the array, also expressed in decibels.

To ensure the stability of the sound source throughout the measurements, a Brüel & Kjær Type 2250 Light Hand-Held Sound Frequency Analyzer was placed at a fixed reference point within the anechoic chamber (see Fig. 4). This device monitored continuously the level of the sound source to allow a source stability correction in the event of a slight change in the loudspeaker's power efficiency.

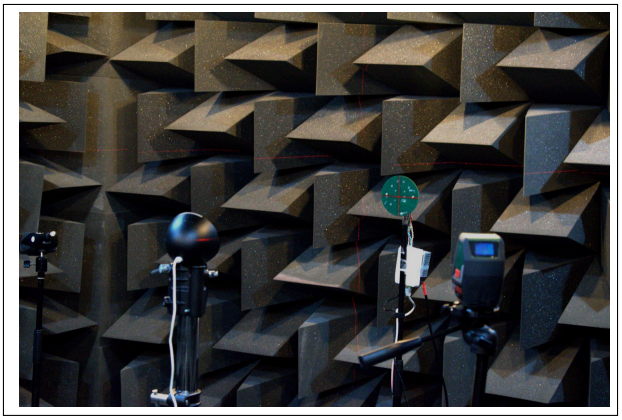

Figure 3. Cross-line laser positioning to maintain the measurement spot at 1 m from the sound source. In the picture, the laser aims at the central microphone of the concentric array.

In the second procedure, the microphone array was positioned at a greater distance of 2.5 m from the sound source. The purpose of this measurement was to assess the collective response of the array, assuming that at this distance, the sound waves would approximate a plane wavefront, meaning that all microphones would receive the signal with minimal differences in amplitude and frequency content due to source directivity. This measurement approach allowed for the characterization of the array's response under conditions where spatial variations in the sound field were minimized, avoiding an iterative relocation of the array. All the recorded signals from the microphones were compared to determine variations in frequency response across the array and to evaluate the consistency of microphone performance.

Figure 4. SGA positioned at one meter from the sound source. A sound frequency analyzer was placed at a fixed position to control the sound source's stability.

3.2 Directivity

The directivity of both microphone arrays was measured by rotating the array in 30-degree increments relative to the sound source in the horizontal plane. The sound-receiver distance was marked at 2.5 m. The frequency response at each angle was normalized by the response measured at 0 degrees (frontal incidence), representing the direction of maximum sensitivity [8]. Specifically, we define the directivity function $D(\phi, f)$, quantified in decibels, as

$$D(\phi, f) = H_{\text{av}}(\phi, f)\ (\text{dB}) - H_{\text{av}}(0^\circ, f)\ (\text{dB}), \qquad (2)$$

where $H_{\text{av}}(\phi, f)$ is the average of the frequency response magnitudes across all microphones at a specific rotational angle ϕ and frequency f, expressed in decibels. The term, $H_{\text{av}}(0^\circ, f)$, represents the reference response measured when the microphone cavities and PCB orifices directly face the sound source ($\phi = 0^\circ$), also in decibels.

3.3 Time-Division Multiplexing Synchronization

An additional experiment was conducted to validate the integrity of the TDM acquisition process and the phase response of the microphones, which consisted of placing the microphone array at a distance of 2.5 m from the sound source, emitting a low-frequency tone through the speaker. Thus, potential time delays between channels can be visualized by comparing the recorded signals across

the microphones. Since the TDM protocol transmits microphone signals sequentially, a key concern was whether the multiplexing process introduced any artifacts or synchronization errors by analyzing the phase alignment of the recorded signals.

4. RESULTS

4.1 Microphone Frequency Response

All presented spectral results were processed using one-third octave band filtering for a clearer comparison and interpretation.

As detailed in 3.1, the individual microphone response was captured at a time and compared to the average, as Equation (1) indicates. Figure 5 displays the range of values in which all the frequency responses are found, observed across the entire set of microphones, as well as selected examples from individual microphones of the CCA. For the SGA, the same experiment was performed for each of its 16 microphones, whose results are displayed in Figure 6.

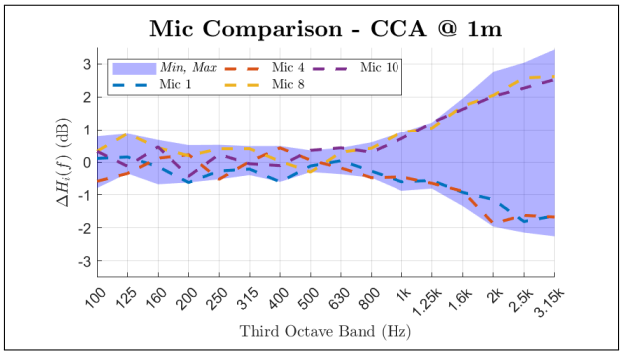

Figure 5. Comparison of the Frequency Response of microphones 1, 4, 8, and 10 of the CCA placed at 1 m from the source. The purple region corresponds to the minimum and maximum frequency response values.

Fig. 7 shows the frequency response evaluated following our second procedure. In this case, with the array positioned at 2.5 m from the source, all microphones were assessed simultaneously, under conditions approximating a plane wavefront. It is important to note that this second procedure was carried out as an alternative to the first one, aiming to reduce its associated uncertainty due to its iterative process which involves the array repositioning for each microphone, and that could be affected by small

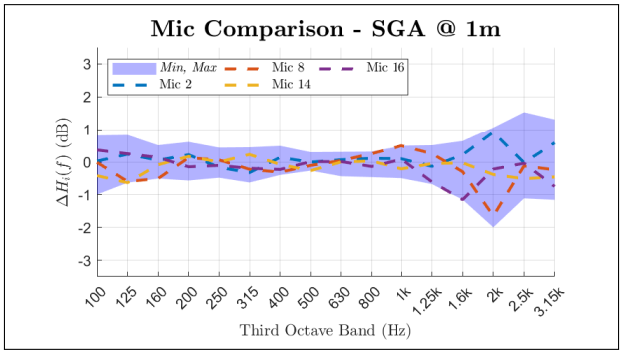

Figure 6. Comparison of the individual frequency response of microphones 2, 8, 14, and 16 of the SGA placed at 1 m from the source. The purple region corresponds to the minimum and maximum frequency response values.

changes in the source stability. For this reason, we only present here the results for the SGA.

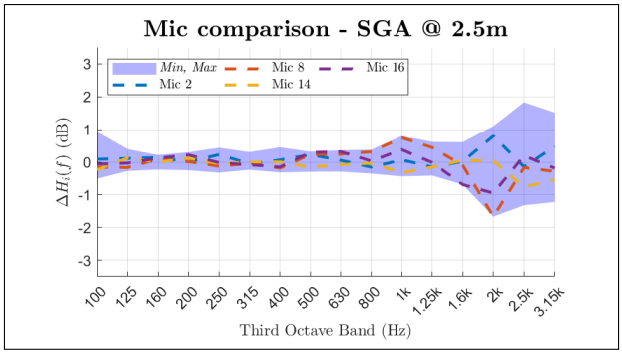

Figure 7. Comparison of the simultaneous frequency response of microphones 2, 8, 14, and 16 of the SGA placed at 2.5 m from the source. The purple region corresponds to the minimum and maximum frequency response values.

4.2 Directivity

The directivity measurement was carried out rotating both arrays in 30° increments over the horizontal axis, keeping a fixed 2.5 m distance to the sound source. The 0° orientation was used as the reference since it aligns with the main axis of sensitivity, as stated in (2). Figures 8 and 9 show the difference between the average response relative

to the reference direction and the rotation angle of ϕ for the CCA and SGA, respectively. Four selected frequency bands are also displayed to ease the visualization.

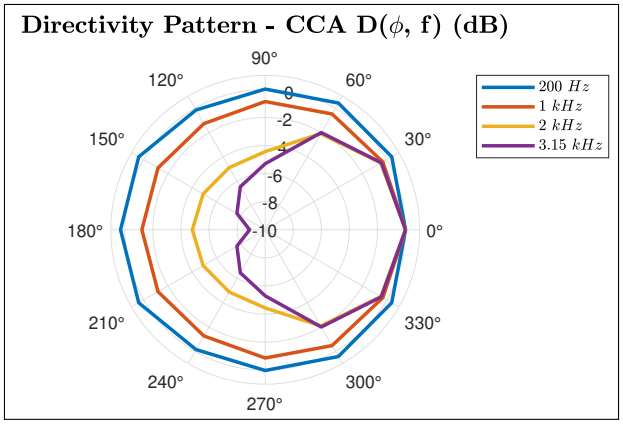

Figure 8. Directivity pattern of the frequency response of the CCA, measured at 2.5 m for the 1/3 octave bands of 200 Hz, 1 kHz, 2 kHz, and 3.15 kHz.

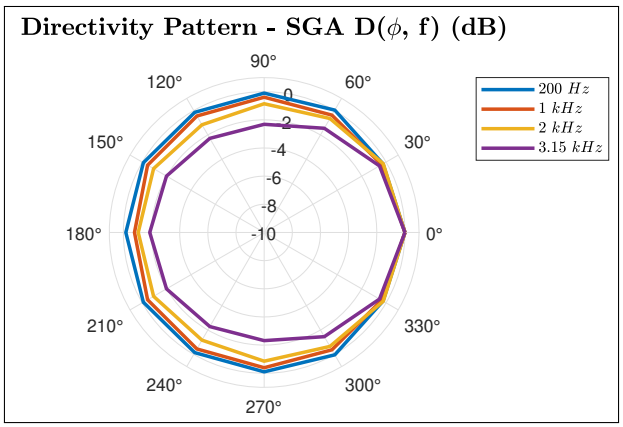

Figure 9. Directivity pattern of the frequency response of the SGA, measured at 2.5 m for the 1/3 octave bands of 200 Hz, 1 kHz, 2 kHz, and 3.15 kHz.

4.3 TDM Synchronization

The integrity of the TDM data acquisition system was examined using a low-frequency signal, which has to be at least higher than the anechoic chamber cut-off frequency, i.e., above 143 Hz. Two sinusoidal signals were tested at 200 Hz and 500 Hz, chosen for its relatively long period (5 ms and 2 ms respectively) compared to the sampling interval (125 µs at the 8 kHz sampling rate). Given that the SGA poses the worst-case scenario, with 16 audio channels and the longest data line traces, it was chosen for this test. The array was positioned at 2.5 m, minimizing the paths differences with respect to the wavelength. To quantify synchronization offsets $\Delta(\tau)$, the signal from each microphone channel was compared against the signal from microphone 1, which served as a stable reference for being the first channel in the TDM data stream. This comparison was performed using a cross-correlation calculated over sliding windows of 600 samples. The analysis was systematically swept along the entire signal length for all microphones. Fig. 10 presents the results of this analysis at 200 Hz, only plotting the calculated time delay evolution of the reference microphone and any detected to be off-sync. For the test using 500 Hz signal, no off-sync was detected.

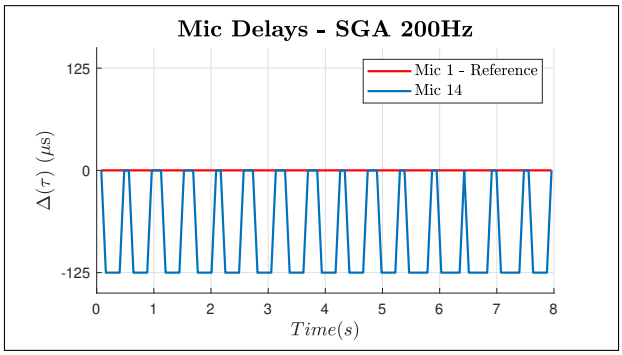

Figure 10. Delay pattern over time using a 200 Hz signal with SGA. Delays are shown in steps of 125 µs due to the sample frequency employed in this acquisition.

As can be seen, only channel 14 shows a fluctuation in synchronization, appearing to drift in and out of phase alignment with the reference channel. Fig. 11 provides a snapshot in the time domain, illustrating a moment when microphone 14's signal is visibly delayed compared to microphone 1, confirming the detected synchronization drift.

5. DISCUSSION AND CONCLUSIONS

This study presents an experimental evaluation of two microphone array prototypes (CCA and SGA), developed using identical MEMS sensor models and the same data transmission protocol to the same BeagleBone Black

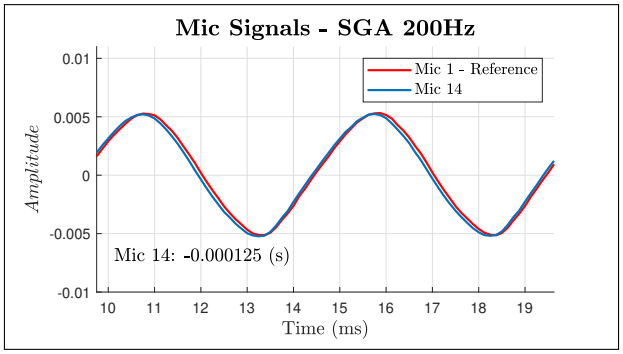

Figure 11. Snapshot in the time domain of waveforms from microphones 1 and 14 when desynchronized. Note that both are overlaid at the moment where the difference becomes most evident.

board, in order to ensure a fair and consistent comparison. The characterization experiments demonstrated the overall functional performance of both the CCA and SGA. Individual microphone frequency responses showed good consistency across both arrays, particularly within the stable 100 Hz to 1 kHz range. Minor deviations observed at higher frequencies are likely due to small positioning variations and inherent microphone differences, while the CCA's response above 1 kHz suggested additional scattering effects, possibly influenced by its solid central mounting board. This structural component may introduce diffraction or reflection that becomes more relevant as frequency increases.

Comparing the former procedure with measurements taken at 2.5 m with SGA, results show a similar behavior, with an even more uniform frequency response, especially when compared to sequential measurements taken at 1 m. Rather than thinking in different frequency responses depending on the distance, we consider that this difference could be caused by a reduced uncertainty in the procedure because of simultaneous measurements that avoids the reallocation of the array and prevent small fluctuations in the emitted sound power of the source. Nevertheless, small differences remained at higher frequencies, indicating that individual microphone characteristics still play a role even under more ideal conditions.

Directivity analysis allows concluding that SGA exhibits a sensitivity with lower dependency on the angle. This behavior seems related to the construction of the arrays (solid design for CCA vs grid structure for SGA). In fact, for the CCA, rotation in 30º increments revealed significant attenuation of high-frequency content when the array was turned around 180º from the source. These results underline the impact of array geometry, construction, and orientation, particularly in aeroacoustic environments where source directionality is a key factor.

The TDM synchronization test for SGA using a 200 Hz signal revealed detectable, periodic time delays for at least one channel relative to the reference. While these delays are bounded by the system's sampling step of 125 µs, their presence suggests that in applications requiring very precise phase alignment, such as beamforming or source localization, potential channel-specific compensation must be applied. That said, the overall results showed that the multiplexing process did not introduce significant artifacts, and most microphones remained well-aligned over time, especially those that are at the end of the stream (microphones 15 and 16), which could have been the most delayed. As a conclusion, a deeper study about the delay evaluation should be performed in order to conclude if this behavior is only related to the phase response of the microphone.

In summary, the experiments provide a solid baseline for understanding the operational characteristics of both arrays. While their overall behavior supports their use in typical aeroacoustic applications, special attention should be given to high-frequency variability, directional response, and synchronization fidelity when designing experiments that rely on fine spatial or temporal resolution.

6. ACKNOWLEDGMENTS

This work has been supported by Grant TED2021-130909A-I00, funded by MCIN/AEI/10.13039/501100011033 and by the European Union NextGenerationEU/PRTR.

7. REFERENCES

[1] J. Yan, C. Chen, Z. Wu, X. Ding, and L. Lou, "An acoustic localization sensor based on mems microphone array for partial discharge," *Sensors*, vol. 23, no. 3, 2023.

[2] J. Picaut, A. Can, N. Fortin, J. Ardouin, and M. Lagrange, "Low-cost sensors for urban noise monitoring networks—a literature review," *Sensors*, vol. 20, no. 8, 2020.

[3] I. Hafizovic, C.-I. C. Nilsen, M. Kjølerbakken, and V. Jahr, "Design and implementation of a mems mi-

crophone array system for real-time speech acquisition," *Applied Acoustics*, vol. 73, no. 2, pp. 132–143, 2012.

[4] M. Turqueti, J. Saniie, and E. Oruklu, "Mems acoustic array embedded in an fpga based data acquisition and signal processing system," in *2010 53rd IEEE International Midwest Symposium on Circuits and Systems*, pp. 1161–1164, 2010.

[5] J. O. Narro and R. Moreno, "64-microhpone module for a massive acoustic camera," in *Proc. of the Tecniacustica*, 2024.

[6] Invensense, "ICS-52000 Datasheet."

[7] Z. Prime and C. J. Doolan, "A comparison of popular beamforming arrays," in *Proc. of ACOUSTICS*, 2013.

[8] L. L. Beranek and T. Mellow, *Acoustics: sound fields and transducers*. Academic Press, 2012.